Semiconductive Coordination Networks from 2,3,6,7,10,11-Hexakis(alkylthio)triphenylenes and Bismuth(III) Halides: Synthesis, Structure−Property Relations, and Solution Processing

Kunhao Li, Zhengtao Xu,* Hanhui Xu, and Jacqueline M. Ryan†

Department of Chemistry, The George Washington University, 725 21st Street NW, Washington, DC 20052

Received February 18, 2005. Revised Manuscript Received May 25, 2005

This paper reports our initial efforts to promote electronic communications across polycyclic aromatic molecules through intervening metal halide moieties. Such efforts stand as part of the larger scheme to overcome the limitation of the van der Waals barrier in molecular semiconductors. In particular, the polycyclic aromatic ligands of 2,3,6,7,10,11-hexakis(alkylthio)triphenylene (alkyl: methyl, ethyl, and isopropyl; corresponding abbreviations for the molecules, HMTT, HETT, and HiPTT) were synthesized in an improved method, and interacted with bismuth(III) bromide and chloride to produce in high yields of a series of semiconductive hybrid networks featuring flexible network dimensionalities and electronic properties, as well as promising solution processing properties. Enlarging the side group from methyl to ethyl and to isopropyl groups effectively reduces the dimensionality of the bismuth halide components (and consequently the dimensionality of the overall coordination framework). Solid-state optical absorption measurements indicate effective electronic interactions between the organic π-system and the bismuth trihalide component, and the electronic band gap decreases monotonically with increasing dimensionality of the coordination network. As compared to molecular semiconductors, these integrated hybrid networks feature stronger electronic communication across the organic molecules, and point to potentially higher charge carrier mobilities.

Introduction

A major research area of solid-state electronics is to integrate organic semiconductive materials into electronic devices such as field effect transistors (FETs) and composite solar cells.[1−16] The widely studied organic semiconductors include polymeric/oligomeric systems (e.g., oligothiophenes and oligophenyls)[17−21] and fused aromatics (e.g., pentacene and hexabenzocoronene derivatives).[22−33] Besides their inherent functional flexibility, organic semiconductors can often be dissolved (either directly or through chemical modification) in common solvents for low-temperature

* To whom correspondence should be addressed. E-mail: zxu@gwu.edu.
† GWU Undergraduate Gamow Fellow.

(1) Dimitrakopoulos, C. D.; Malenfant, P. R. L. *Adv. Mater.* **2002**, *14*, 99.
(2) Katz, H. E.; Bao, Z.; Gilat, S. L. *Acc. Chem. Res.* **2001**, *34*, 359.
(3) Forrest, S. R. *Nature* **2004**, *428*, 911.
(4) Katz, H. E.; Bao, Z. *J. Phys. Chem. B* **2000**, *104*, 671.
(5) Bao, Z. *Adv. Mater.* **2000**, *12*, 227.
(6) Kaschak, D. M.; Johnson, S. A.; Waraksa, C. C.; Pogue, J.; Mallouk, T. E. *Coord. Chem. Rev.* **1999**, *185−186*, 403.
(7) Yonemoto, E. H.; Kim, Y. I.; Schmehl, R. H.; Wallin, J. O.; Shoulders, B. A.; Richardson, B. R.; Haw, J. F.; Mallouk, T. E. *J. Am. Chem. Soc.* **1994**, *116*, 10557.
(8) Bose, A.; He, P.; Liu, C.; Ellman, B. D.; Twieg, R. J.; Huang, S. D. *J. Am. Chem. Soc.* **2002**, *124*, 4.
(9) Nishimura, S.; Abrams, N.; Lewis, B. A.; Halaoui, L. I.; Mallouk, T. E.; Benkstein, K. D.; van de Lagemaat, J.; Frank, A. J. *J. Am. Chem. Soc.* **2003**, *125*, 6306.
(10) Hagfeldt, A.; Grätzel, M. *Acc. Chem. Res.* **2000**, *33*, 269.
(11) Bach, U.; Lupo, D.; Comte, P.; Moser, J. E.; Weissörtel, F.; Salbeck, J.; Spreitzer, H.; Grätzel, M. *Nature* **1998**, *395*, 583.
(12) O'Regan, B.; Grätzel, M. *Nature* **1991**, *353*, 737.
(13) Yu, G.; Gao, J.; Hummelen, J. C.; Wudl, F.; Heeger, A. J. *Science* **1995**, *270*, 1789.
(14) McFarland, E. W.; Tang, J. *Nature* **2003**, *421*, 616.
(15) Xue, J.; Uchida, S.; Rand, B. P.; Forrest, S. R. *Appl. Phys. Lett.* **2004**, *84*, 3013.
(16) Peumans, P.; Uchida, S.; Forrest, S. R. *Nature* **2003**, *425*, 158.
(17) Facchetti, A.; Deng, Y.; Wang, A.; Koide, Y.; Sirringhaus, H.; Marks, T. J.; Friend, R. H. *Angew. Chem., Int. Ed.* **2000**, *39*, 4547.
(18) Mushrush, M.; Facchetti, A.; Lefenfeld, M.; Katz, H. E.; Marks, T. J. *J. Am. Chem. Soc.* **2003**, *125*, 9414.
(19) Facchetti, A.; Yoon, M.-H.; Stern, C. L.; Katz, H. E.; Marks, T. J. *Angew. Chem., Int. Ed.* **2003**, *42*, 3900.
(20) Sirringhaus, H.; Brown, P. J.; Friend, R. H.; Nielsen, M. M.; Bechgaard, K.; Langeveld-Voss, B. M. W.; Spiering, A. J. H.; Janssen, R. A. J.; Meijer, E. W.; Herwig, P.; de Leeuw, D. M. *Nature* **1999**, *401*, 685.
(21) Gundlach, D. J.; Lin, Y. Y.; Jackson, T. N.; Schlom, D. G. *Appl. Phys. Lett.* **1997**, *71*, 3853.
(22) Meng, H.; Bendikov, M.; Mitchell, G.; Helgeson, R.; Wudl, F.; Bao, Z.; Siegrist, T.; Kloc, C.; Chen, C.-H. *Adv. Mater.* **2003**, *15*, 1090.
(23) Watson, M. D.; Fechtenkötter, A.; Müllen, K. *Chem. Rev.* **2001**, *101*, 1267.
(24) Dimitrakopoulos, C. D.; Purushothaman, S.; Kymissis, J.; Callegari, A.; Shaw, J. M. *Science* **1999**, *283*, 822.
(25) Afzali, A.; Dimitrakopoulos, C. D.; Breen, T. L. *J. Am. Chem. Soc.* **2002**, *124*, 8812.
(26) Afzali, A.; Dimitrakopoulos, C. D.; Graham, T. O. *Adv. Mater.* **2003**, *15*, 2066.
(27) Sheraw, C. D.; Jackson, T. N.; Eaton, D. L.; Anthony, J. E. *Adv. Mater.* **2003**, *15*, 2009.
(28) Miao, Q.; Nguyen, T.-Q.; Someya, T.; Blanchet, G. B.; Nuckolls, C. *J. Am. Chem. Soc.* **2003**, *125*, 10284.
(29) Gundlach, D. J.; Lin, Y. Y.; Jackson, T. N.; Nelson, S. F.; Schlom, D. G. *IEEE Electron Device Lett.* **1997**, *18*, 87.
(30) Shtein, M.; Mapel, J.; Benziger, J. B.; Forrest, S. R. *Appl. Phys. Lett.* **2002**, *81*, 268.
(31) van de Craats, A. M.; Stutzmann, N.; Bunk, O.; Nielsen, M. M.; Watson, M.; Müllen, K.; Chanzy, H. D.; Sirringhaus, H.; Friend, R. H. *Adv. Mater.* **2003**, *15*, 495.
(32) Debije, M. G.; Piris, J.; De Haas, M. P.; Warman, J. M.; Tomovic, Z.; Simpson, C. D.; Watson, M. D.; Müllen, K. *J. Am. Chem. Soc.* **2004**, *126*, 4641.
(33) Xue, J.; Forrest, S. R. *Appl. Phys. Lett.* **2001**, *79*, 3714.

10.1021/cm050377+ CCC: $30.25
Published on Web 07/30/2005

Scheme 1

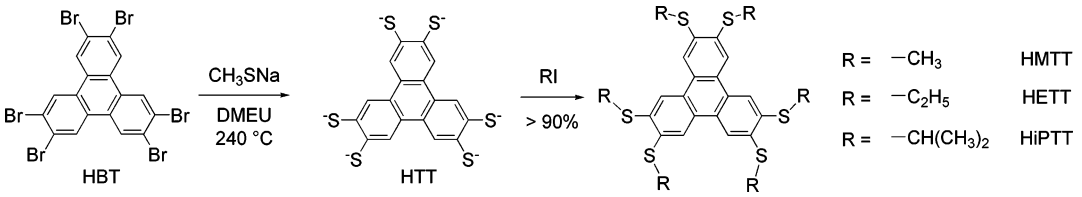

processing, thus offering great potential for large-area, flexible electronics applications. One major limitation of organic semiconductors, however, is the considerably lower charge carrier mobilities (as compared to the covalent inorganic systems such as Si, Ge, and GaAs), which is fundamentally imposed by the weak van der Waals interactions between organic molecules. In fact, the major charge transport pathway in organic semiconductors is generally considered to be along the direction of maximum $\pi-\pi$ orbital overlap between the organic molecules.[34,35]

By comparison, coordination bonds, with their intermediate strength between covalent and van der Waals interactions, could potentially provide an intermolecular linkage to overcome the van der Waals barrier of molecular semiconductors, while preserving the solution processability at the same time. Among the rapidly growing number of metal−organic coordination networks,[36−40] however, conductive or semiconductive systems[38,41−48] remain relatively rare. The crux here is that the organic ligands usually are of low electroactivity, and their electronic communications with the metal centers are quite weak. Recently, redox-active molecules such as tetrathiafulvalene (TTF) and its derivatives have been equipped with chelating sites such as the phosphine[49−52] and organylthio[43−45] groups, thus offering an avenue to potentially stronger electronic interaction between the ligand and the metal center. Besides the air sensitivity commonly associated with the TTF moiety, metal−organic complexes thus formed usually consist of isolated molecular species[45,49,51,53,54] or networks based on relatively "inert" ions such as Ag^+ or Cu^+.[43,55−57] It thus remains a challenging task to achieve crystalline coordination networks with prevalent electronic communication between the ligand and the metal center, especially networks with demonstrated solution processability and air stability.

We here report a class of semiconductive hybrid networks that may point to a rather versatile synthetic approach to tackle the issues regarding metal−ligand interaction, solution processability, and air stability. Generally, this is an approach based upon the interaction between metal halides and polycyclic aromatic molecules containing multiple chelation groups. Specifically, we have interacted bismuth(III) halides (chloride and bromide) with the ligands of 2,3,6,7,10,11-hexakis(alkylthio)triphenylene (alkyl, methyl, ethyl, and isopropyl; corresponding abbreviations for the molecules, HMTT, HETT, and HiPTT, see also Scheme 1). The triphenylene core is selected here mainly for the following reasons: (1) it has a large, polarizable fused π-electron system to enhance the electroactivity of the resultant network; and (2) its symmetric structure can readily accommodate three pairs of 1,2-bis(alkylthio) groups (e.g., those in HMTT, HETT, and HiPTT), which can chelate[44,58−60] metal ions to enhance the electronic interactions between the organic π system and the metal center. Incidentally, symmetrically substituted triphenylene molecules are generally stable in air and have been widely studied for their discotic liquid crystalline properties[61−64] and as potential molecular semiconductors.[34,65]

Additionally, the bismuth(III) halides could provide the following potential advantages. First, Bi(III) is slightly oxidative and may serve as an electron acceptor for the

(34) Boden, N.; Bushby, R. J.; Clements, J.; Movaghar, B.; Fonobsn, K. J.; Kreouzis, T. *Phys. Rev. B: Condens. Matter* **1995**, *52*, 13274.
(35) van de Craats, A. M.; Warman, J. M. *Adv. Mater.* **2001**, *13*, 130.
(36) Batten, S. R.; Robson, R. *Angew. Chem., Int. Ed.* **1998**, *37*, 1461.
(37) Yaghi, O. M.; O'Keeffe, M.; Ockwig, N. W.; Chae, H. K.; Eddaoudi, M.; Kim, J. *Nature* **2003**, *423*, 705.
(38) Janiak, C. *Dalton Trans.* **2003**, 2781.
(39) James, S. L. *Chem. Soc. Rev.* **2003**, *32*, 276.
(40) Kesanli, B.; Lin, W. *Coord. Chem. Rev.* **2003**, *246*, 305.
(41) Hanack, M.; Deger, S.; Lange, A. *Coord. Chem. Rev.* **1988**, *83*, 115.
(42) Kato, R. *Bull. Chem. Soc. Jpn.* **2000**, *73*, 515.
(43) Zhong, J. C.; Misaki, Y.; Munakata, M.; Kuroda-Sowa, T.; Maekawa, M.; Suenaga, Y.; Konaka, H. *Inorg. Chem.* **2001**, *40*, 7096.
(44) Inoue, M. B.; Inoue, M.; Bruck, M. A.; Fernando, Q. *Chem. Commun.* **1992**, 515.
(45) Gan, X.; Munakata, M.; Kuroda-Sowa, T.; Maekawa, M. *Bull. Chem. Soc. Jpn.* **1994**, *67*, 3009.
(46) Aumüller, A.; Erk, P.; Klebe, G.; Hünig, S.; Schütz, J. U. v.; Werner, H.-P. *Angew. Chem., Int. Ed. Engl.* **1986**, *25*, 740.
(47) Kato, R.; Kobayashi, H.; Kobayashi, A. *J. Am. Chem. Soc.* **1989**, *111*, 5224.
(48) Heintz, R. A.; Zhao, H. H.; Xiang, O. Y.; Grandinetti, G.; Cowen, J.; Dunbar, K. R. *Inorg. Chem.* **1999**, *38*, 144.
(49) Smucker, B. W.; Dunbar, K. R. *Dalton Trans.* **2000**, 1309.
(50) Fourmigué, M.; Uzelmeier, C. E.; Boubekeur, K.; Bartley, S. L.; Dunbar, K. R. *J. Organomet. Chem.* **1997**, *529*, 343.
(51) Uzelmeier, C. E.; Bartley, S. L.; Fourmigué, M.; Rogers, R.; Grandinetti, G.; Dunbar, K. R. *Inorg. Chem.* **1998**, *37*, 6706.
(52) Asara, J. M.; Uzelmeier, C. E.; Dunbar, K. R.; Allison, J. *Inorg. Chem.* **1998**, *37*, 1833.
(53) Avarvari, N.; Fourmigué, M. *Chem. Commun.* **2004**, 1300.
(54) Cerrada, E.; Diaz, C.; Diaz, M. C.; Hursthouse, M. B.; Laguna, M.; Light, M. E. *J. Chem. Soc., Dalton Trans.* **2002**, 1104.
(55) Munakata, M.; Kuroda-Sowa, T.; Maekawa, M.; Hirota, A.; Kitagawa, S. *Inorg. Chem.* **1995**, *34*, 2705.
(56) Gan, X.; Munakata, M.; Kuroda-Sowa, T.; Maekawa, M.; Misaki, Y. *Polyhedron* **1995**, *14*, 1343.
(57) Yamamoto, M.; Gan, X.; Kuroda-Sowa, T.; Maekawa, M.; Suenaga, Y.; Munakata, M. *Inorg. Chim. Acta* **1997**, *261*, 169.
(58) Suenaga, Y.; Kuroda-Sowa, T.; Munakata, M.; Maekawa, M.; Morimoto, H. *Polyhedron* **1998**, *18*, 429.
(59) Suenaga, Y.; Kuroda-Sowa, T.; Maekawa, M.; Munakata, M. *Dalton Trans.* **2000**, 3620.
(60) Suenaga, Y.; Konaka, H.; Kitamura, K.; Kuroda-Sowa, T.; Maekawa, M.; Munakata, M. *Inorg. Chim. Acta* **2003**, *351*, 379.
(61) Billard, J.; Dubois, J. C.; Tinh, N. H.; Zann, A. *Nouv. J. Chim.* **1978**, *2*, 535.
(62) Lee, W. K.; Heiney, P. A.; McCauley, J. P., Jr.; Smith, A. B., III. *Mol. Cryst. Liq. Cryst.* **1991**, *198*, 273.
(63) Destrade, C.; Mondon, M. C.; Malthete, J. *J. Phys. (Paris) Colloq.* **1979**, *40*, 17.
(64) Demus, D.; Goodby, J.; Gray, G. W.; Spiess, H. W.; Vill, V. *Handbook of Liquid Crystals*; Wiley-VCH Verlag: Weinheim, 1998.
(65) Boden, N.; Bushby, R. J.; Clements, J.; Movaghar, B. *J. Mater. Chem.* **1999**, *9*, 2081.

Table 1. Selected Crystallographic Data for HMTT·$BiBr_3$ (2), HMTT·$2BiBr_3$ (3), HETT·$2BiBr_3$ (4), and HiPTT·$2BiBr_3$·C_7H_8 (5)

	2	3	4	5
chem. formula	$C_{24}H_{24}BiBr_3S_6$	$C_{24}H_{24}Bi_2Br_6S_6$	$C_{30}H_{36}Bi_2Br_6S_6$	$C_{86}H_{112}Bi_4Br_{12}S_{12}$
fw	953.50	1402.21	1486.37	3325.32
space group	$P\bar{1}$	$P\bar{1}$	$P\bar{1}$	$P2_1/c$
a, Å	8.0012(1)	12.2882(2)	8.9547(1)	32.1249(3)
b, Å	14.1769(2)	12.5597(1)	14.8258(1)	16.0700(2)
c, Å	14.1819(2)	13.0650(2)	16.5651(2)	22.8463(2)
α, deg	108.0052(5)	71.5783(5)	103.9694(4)	90
β, deg	99.8834(5)	86.4844(4)	100.3993(4)	96.4605(3)
γ, deg	97.6791(5)	68.5989(5)	94.5313(6)	90
V, Å^3	1476.98(3)	1777.84(4)	2081.71(4)	11 719.4(2)
Z	2	2	2	4
ρ_{calcd}, g/cm^3	2.144	2.619	2.371	1.885
wavelength, Å	0.71073 (Mo Kα)	0.71073 (Mo Kα)	0.71073 (Mo Kα)	0.71073 (Mo Kα)
abs coeff (μ), cm^{-1}	104.65	169.96	145.23	103.30
R_1[a]	3.83% [$I > 2\sigma(I)$]	4.10% [$I > 2\sigma(I)$]	5.75% [$I > 2\sigma(I)$]	7.71% [$I > 2\sigma(I)$]
wR_2[b]	9.45% [$I > 2\sigma(I)$]	9.44% [$I > 2\sigma(I)$]	15.01% [$I > 2\sigma(I)$]	18.03% [$I > 2\sigma(I)$]

[a] $R_1 = \sum(|F_o| - |F_c|)/\sum(|F_o|)$. [b] $wR2 = \{\sum[w(F_o^2 - F_c^2)^2]/\sum[w(F_o^2)^2]\}^{1/2}$.

aromatic π-system, thus facilitating charge transfer between the organic and inorganic components. Second, as a heavy p-block element, Bi(III) tends to display a high coordination number, especially in halide compounds, where secondary Bi−X (X: halogen atoms) interactions[66,67] often furnish a seven-fold (or higher) coordination sphere around the Bi center. Such a high coordination number promotes the formation of extended networks in the solid state, generating more extensive interconnections across the organic molecules. In addition, hybrid networks involving metal−halogen bonds[68−81] tend to be more soluble in organic solvents than other inorganic compounds such as chalcogenides, and can help maintain processability[78−81] in organic solvents.

The study here uncovers a series of hybrid semiconductive networks that simultaneously incorporate two types of coordination bonds: the ones between the organic molecules and the Bi(III) centers (i.e., Bi−S) and the ones between the Bi(III) and the halogen atoms (i.e., Bi−X). The coordination networks feature variable dimensionalities encompassing isolated hybrid units, quasi-1D, 1D, and 2D systems. The dimensionalities of the networks can be modified by the size of the alkyl side chains of the organic molecules as well as by the organic molecule/bismuth trihalide ratio. More importantly, structure−electronic property studies identify strong correlation between electronic band gap and the dimensionality of the coordination network, suggesting the Bi−S and Bi−X coordination bonds as potentially significant determinants of the solid-state electronic properties. In other words, these coordination bonds could potentially parallel or overtake the van der Waals interaction as a major interconnecting force that mediates the electronic interaction across the organic molecules. Also, the hybrid networks are convenient to form, generally stable to air, and several of them are found to be amenable to solution deposition, suggesting potential applications for semiconductive device fabrication (e.g., in field effect transistors).

Experimental Section

General Procedure. Starting materials, reagents, and solvents were purchased from commercial sources (Aldrich and Fisher Scientific) and used without further purification. Melting points were measured on a Mel-temp II melting point apparatus. Solution ^{1}H and ^{13}C NMR spectra were taken on a 200 MHz Varian Mercury spectrometer at room temperature, with tetramethylsilane (TMS) as the internal standard.

X-ray datasets of the single-crystal samples were collected on a Nonius kappaCCD system using Mo Kα ($\lambda = 0.71073$ Å) radiation at 293(2) K. The absorption effects were minimized by scaling and averaging of redundant measurements. The structures were solved and refined by full-matrix least-squares on F_o^2 using SHELXL 97. Selected crystallographic data are summarized in Table 1. X-ray diffraction patterns for the bulk samples as well as the solution-deposited crystallites were collected at room temperature on a Scintag XDS 2000 diffractometer (Cu Kα, $\lambda = 1.5418$ Å). The powder samples were pressed onto a glass slide for data collection. A 2θ range of 3−50° was collected. The program JADE (Materials Data, Inc.) was used in the calculation of powder patterns from single-crystal structures.

Optical diffuse reflectance measurements were performed at room temperature with a JASCO V-570 double-beam, single-monochromator spectrophotometer in the 350−1500 nm region. The instru-

(66) Starbuck, J.; Norman, N. C.; Orpen, A. G. *New J. Chem.* **1999**, *23*, 969.
(67) Alcock, N. W. *Adv. Inorg. Chem. Radiochem.* **1972**, *15*, 1.
(68) (a) Barton, A. J.; Genge, A. R. J.; Levason, W.; Reid, G. *Dalton Trans.* **2000**, 2163. (b) Barton, A. J.; Hill, N. J.; Levason, W.; Reid, *Dalton Trans.* **2001**, 1621. (c) Genge, A. R. J.; Hill, N. J.; Levason, W.; Reid, G. *Dalton Trans.* **2001**, 1007. (d) Hill, N. J.; Levason, W.; Reid, G. *Inorg. Chem.* **2002**, *41*, 2070. (e) Levason, W.; Hill, N. J.; Reid, G. *Dalton Trans.* **2002**, 4316. (f) Hill, N. J.; Levason, W.; Patel, R.; Reid, G.; Webster, M. *Dalton Trans.* **2004**, 980.
(69) (a) Martin, J. D.; Greenwood, K. B. *Angew. Chem. Int. Ed. Engl.* **1997**, *36*, 2072. (b) Martin, J. D.; Leafblad, B. R. *Angew. Chem. Int. Ed.* **1998**, *37*, 3318.
(70) Martin, J. D.; Hess, R. F.; Boyle, P. D. *Inorg. Chem.* **2004**, *43*, 3242.
(71) Julve, M.; De Munno, G.; Bruno, G.; Verdaguer, M. *Inorg. Chem.* **1988**, *27*, 3160.
(72) Loï, M.; Graf, E.; Hosseini, M. W.; De Cian, A.; Fischer, J. *Chem. Commun.* **1999**, 603.
(73) Neels, A.; Neels, B. M.; Stoeckli-Evans, H.; Clearfield, A.; Poojary, D. M. *Inorg. Chem.* **1997**, *36*, 3402.
(74) Ferigo, M.; Bonhote, P.; Marty, W.; Stoeckli-Evans, H. *J. Chem. Soc., Dalton Trans.* **1994**, 1549.
(75) Rogers, R. D.; Bond, A. H.; Wolff, J. L. *J. Coord. Chem.* **1993**, *29*, 187.
(76) Bowmaker, G. A.; Harrowfield, J. M.; Miyamae, H.; Shand, T. M.; Skelton, B. W.; Soudi, A. A.; White, A. H. *Aust. J. Chem.* **1996**, *49*, 1089.
(77) Harrowfield, J. M.; Miyamae, H.; Shand, T. M.; Skelton, B. W.; Soudi, A. A.; White, A. H. *Aust. J. Chem.* **1996**, *49*, 1043.
(78) Xu, C. Q.; Kondo, T.; Sakakura, H.; Kumata, K.; Takahashi, Y.; Ito, R. *Solid State Commun.* **1991**, *79*, 245.
(79) Kagan, C. R.; Mitzi, D. B.; Dimitrakopoulos, C. D. *Science* **1999**, *286*, 945.
(80) Mitzi, D. B. *Prog. Inorg. Chem.* **1999**, *48*, 1.
(81) Xu, Z.; Mitzi, D. B. *Chem. Mater.* **2003**, *15*, 3632.

ment was equipped with an integrating sphere. $BaSO_4$ powder was used as reference (100% reflectance). Absorption data α/S (α, absorption coefficient; S, scattering factor) were calculated from the reflectance data using the Kubelka−Munk function. The band gap was determined as the intersection point between the energy axis at the absorption offset and the line extrapolated from the sharp absorption edge in the α/S versus E (eV) plot. The solid sample was finely ground and pressed between two Mylar tapes (sample thickness is ∼1 mm and much greater than the particle size, and therefore an ideal diffuse reflection can be assumed). The sample was held against a white background for data collection.

2,3,6,7,10,11-Hexakis(methylthio)triphenylene (HMTT). The synthesis and characterization of HMTT was described in the Supporting Information of a previous paper.[82]

2,3,6,7,10,11-Hexakis(ethylthio)triphenylene (HETT). In an argon atmosphere, a 50 mL three-neck round-bottom flask was charged with hexabromotriphenylene[83] (HBT, 0.30 g, 0.43 mmol) and sodium thiomethoxide (0.76 g, 95%, 10.3 mmol), and then equipped with a condenser. DMEU (1,3-dimethyl-2-imidazolidinone, anhydrous, 40 mL) was added to the above reagents via cannula, and the reaction mixture was heated at a refluxing temperature (∼240 °C) under argon for 6 h. The reaction mixture was then cooled to room temperature, and iodoethane (99% purity, pre-purged with argon for 5 min, 2.0 mL, 25 mmol) was added to the greenish yellow suspension. After 30 min, the reaction mixture was poured into 150 mL of water and the precipitate was filtered, washed with water (100 mL × 3), and dried under vacuum. The purity of the product thus obtained (0.25 g, beige, 100% based on HBT) was checked by ^{1}H and ^{13}C NMR and the melting point. Melting point: 189−190 °C. ^{1}H NMR (200 MHz, $CDCl_3$): δ 1.46 (t, 18H, J = 7.4 Hz), 3.14 (q, 12H, J = 7.4 Hz), 8.29 (s, 6H). ^{13}C NMR (50 MHz, $CDCl_3$): δ 14.14, 28.00, 123.24, 127.48, 136.95. The product was further purified by a silica gel column (CH_2Cl_2/hexane 1:4) before being used for crystal growth with $BiBr_3$.

2,3,6,7,10,11-Hexakis(isopropylthio)triphenylene (HiPTT). Under argon protection, hexabromotriphenylene (0.40 g, 0.57 mmol) and sodium thiomethoxide (1.00 g, 95%, 13.6 mmol) were loaded into a 50 mL three-neck round-bottom flask, and the flask was then connected to a condenser. DMEU (anhydrous, 40 mL) was transferred into the flask via cannula, and the reaction mixture was heated at refluxing for 6 h. Thereafter, the reaction mixture was cooled to 70 °C, and 2-iodopropane (99% purity, pre-purged with argon for 5 min, 2.8 mL, 27.7 mmol) was injected into the greenish yellow suspension. After being stirred for 1 h, the reaction mixture was poured into 200 mL of ice water and extracted by toluene (100 mL × 3). The toluene solution was then washed with water (200 mL × 3) and brine (saturated, 200 mL), dried over sodium sulfate, and evaporated in vacuo to afford a light yellow solid (0.38 g, 99% based on HBT). The purity of the product thus obtained was checked by ^{1}H and ^{13}C NMR and the melting point. Melting point: 124−126 °C. ^{1}H NMR (200 MHz, $CDCl_3$): δ 1.45 (d, 36H, J = 6.4 Hz), 3.69 (septet, 6H, J = 6.4 Hz), 8.42 (s, 6H). ^{13}C NMR (50 MHz, $CDCl_3$): δ 23.06, 37.74, 125.30, 127.72, 137.46. The product was further purified by a silica gel column (CH_2Cl_2/hexane 1:4) before being used for crystal growth with $BiBr_3$.

Crystallization of HMTT·$BiCl_3$ (1). The synthesis and characterization of this compound has been previously reported.[82]

Crystallization of HMTT·$BiBr_3$ (2). The single-crystal structure was obtained from samples prepared as follows. HMTT (9.2 mg, 0.018 mmol) and $BiBr_3$ (9.0 mg, 0.020 mmol) in DCB (1,2-dichlorobenzene, anhydrous, 0.6 mL) were loaded into a heavy-wall borosilicate glass tube (Kimax, $^1/_2$ in. OD) in an argon-filled glovebox. The tube was sealed under vacuum (with the reagents being chilled by liquid nitrogen) and heated in a programmable oven at 180 °C for 12 h, followed by slow cooling at 0.1 °C/min to room temperature. Dark-red, blocklike crystals formed in this process, together with a small amount of lighter-colored crystallites. A crystal was selected among the darker (red) ones for X-ray dataset collection, which provided the crystal structure of HMTT·$BiBr_3$ (**2**). Bulk samples of HMTT·$BiBr_3$ (**2**) with single-phase purity can be prepared by dissolving HMTT (11.2 mg, 0.022 mmol) and $BiBr_3$ (11.2 mg, 0.025 mmol) in anhydrous DCB (4 mL) under argon protection at about 180 °C, and then cooling to room temperature over a period of about 30 min (e.g., in an oil bath). This heat-and-cool process was repeated two more times. The dark-red, block-shaped crystallites thus formed were filtered, washed with benzene under argon protection (yield: 18.4 mg, 87% based on HMTT), and subjected to X-ray powder diffraction study, which indicated a single phase consistent with the single-crystal structure of HMTT·$BiBr_3$ (**2**) (see Supporting Information). No degradation of the X-ray diffraction data was observed after overnight, indicating substantial air stability of the powder sample. Chemical analysis of the product $C_{24}H_{24}S_6BiBr_3$ yields the following: calcd [C (30.23%), H (2.54%), S (20.18%), Br (25.14%)]; found [C (30.32%), H (2.61%), S (19.92%), Br (24.95%)].

Crystallization of HMTT·2$BiBr_3$ (3). The single-crystal structure was obtained from samples prepared as follows. HMTT (18.6 mg, 0.037 mmol), $BiBr_3$ (27.8 mg, 0.062 mmol), together with benzene (2.0 mL, anhydrous) were loaded into a heavy-wall borosilicate glass tube (Kimax, $^1/_2$ in. OD). The tube was then sealed under vacuum (with the reagents being chilled by liquid nitrogen) and heated in an oil bath at 150 °C for 8 h, during which dark red, blocklike single crystals suitable for single-crystal X-ray diffraction study were obtained. Bulk samples of HMTT·2$BiBr_3$ (**3**) with single-phase purity can be prepared by heating a mixture of HMTT (11.5 mg, 0.023 mmol), $BiBr_3$ (30.7 mg, 0.068 mmol), and benzene (anhydrous, 1.1 mL) in a sealed glass tube (Kimax, heavy-wall, $^1/_2$ in. OD) at 120 °C for 5 days and then cooling to room temperature at 0.1 °C/min in a programmable oven. The dark red product was filtered and washed with benzene (29.5 mg, 92% based on HMTT). X-ray powder diffraction indicated a single phase consistent with the single-crystal structure (see Supporting Information). Chemical analysis of the product $C_{24}H_{24}S_6Bi_2Br_6$ yields the following: calcd [C (20.56%), H (1.73%), S (13.72%)]; found [C (20.39%), H (1.78%), S (13.33%)].

Crystallization of HETT·2$BiBr_3$ (4). The single-crystal structure was obtained from samples prepared as follows. HETT (8.7 mg, 0.015 mmol) and $BiBr_3$ (9.9 mg, 0.022 mmol) in 0.6 mL of toluene were loaded into a heavy-wall borosilicate glass tube (Kimax, $^3/_8$ in. OD). The tube was sealed under vacuum (with the reagents being chilled by liquid nitrogen) and heated at 120 °C in oil bath for 12 h, during which red, platelike crystals suitable for single-crystal X-ray diffraction study were obtained. Bulk samples of HETT·2$BiBr_3$ (**4**) with single-phase purity can be obtained by heating a mixture of HETT (20 mg, 0.034 mmol), $BiBr_3$ (39.6 mg, 0.088 mmol), and toluene (anhydrous, 1 mL) in a closed pressure tube (#7, Ace Glass) at 100 °C for 24 h and then cooling to room temperature at 0.1 °C/min; orange-red crystallites of HETT·2$BiBr_3$ (**4**) were obtained (47.5 mg, 94% based on HETT). X-ray powder diffraction indicated a single phase consistent with the single-crystal structure (see Supporting Information). Chemical analysis of the product $C_{30}H_{36}S_6Bi_2Br_6$ yields the following: calcd [C (24.24%), H (2.44%), S (12.94%)]; found [C (24.12%), H (2.50%), S (12.84%)].

(82) Xu, Z.; Li, K.; Fettinger, J. C.; Li, J.; King, M. M. *Cryst. Growth Des.* **2005**, *5*, 423.
(83) Yatabe, T.; Harbison, M. A.; Brand, J. D.; Wagner, M.; Müllen, K.; Samori, P.; Rabe, J. P. *J. Mater. Chem.* **2000**, *10*, 1519.

Crystallization of HiPTT·2BiBr$_3$·C$_7$H$_8$ (5). The single-crystal structure was obtained from samples prepared as follows. HiPTT (19.6 mg, 0.029 mmol) and $BiBr_3$ (14.4 mg, 0.032 mmol) in 0.7 mL of toluene were loaded into a heavy-wall borosilicate glass tube (Kimax, $^3/_8$ in. OD). The tube was sealed under vacuum (with the reagents being chilled by liquid nitrogen) and heated at 100 °C in a programmable oven for 2 h and then cooled at 0.1 °C/min to room temperature. Orange-yellow blocklike crystals suitable for single-crystal X-ray diffraction study were obtained. Bulk samples of HiPTT·2BiBr$_3$·C$_7$H$_8$ (**5**) with single-phase purity can be made by dissolving HiPTT (9.6 mg, 0.014 mmol) and $BiBr_3$ (14.7 mg, 0.033 mmol) in toluene (anhydrous, 0.6 mL) at 100 °C under argon protection, and then cooling to room temperature over a period of about 20 min. The orange-yellow crystals were collected by vacuum filtration (14.5 mg, 65% based on HiPTT). X-ray powder diffraction indicated a single phase consistent with the single-crystal structure (see Supporting Information). Solution ^{1}H NMR (200 MHz, CD_2Cl_2) indicated a 1:1 ratio of the HiPTT and the included toluene molecules: δ 1.47 (d, 36 H, J = 6.8 Hz), 2.34 (s, 3H, toluene $-CH_3$), 3.78 (septet, 6H, J = 6.8 Hz), 7.09−7.28 (m, 5H, toluene $-C_6H_5$), 8.14 (s, 6H).

Solution Deposition of HMTT·BiCl$_3$ (1). Inside an argon-filled glovebox, HMTT (2.7 mg, 0.0053 mmol), $BiCl_3$ (2.0 mg, 0.0063 mmol), 1,2-dichlorobenzene (DCB, anhydrous, 1.0 mL), and a magnetic stirring bar were placed into a vial, which was then capped with a septum, taken out of the glovebox, and connected through a needle to an argon-filled manifold. With a slight positive argon pressure thus maintained, the vial was heated to 190 °C in an oil bath (with stirring), and the mixture turned into a light yellow solution. The septum was then removed, and a small portion of the solution (e.g., ~0.2 mL) was quickly drawn into a pipet (preheated to ~190 °C) and at once dropped onto a quartz disk kept at 150 °C on a hot plate. To minimize exposing the solution to air, the quartz disk was immediately covered by a stem funnel connected to a steady stream of outflowing argon gas. In about 2 min, the solvent was evaporated and dark-red crystallites (blocklike, average size $\approx 0.3 \times 0.1 \times 0.05$ mm^3) were deposited on the quartz disk. X-ray powder diffraction of the solution-deposited sample showed a single, crystalline phase consistent with the single-crystal structure of HMTT·$BiCl_3$ (**1**) (with strong orientation preference of the [0$\bar{1}$1] plane). The crystallites are generally stable in air. Attempts to deposit from a DCB solution of HMTT·$BiCl_3$ (**1**) (i.e., with HMTT and $BiCl_3$ in 1:1 molar ratio) under similar conditions resulted in a considerable amount of white, powdery side product, although a more rigorous exclusion of air (e.g., depositing within a dedicated glovebox) might improve the product purity in future explorations.

Solution Deposition of HMTT·BiBr$_3$ (2). HMTT (2.9 mg, 0.0057 mmol) and $BiBr_3$ (5.7 mg, 0.0127 mmol) were dissolved in DCB (anhydrous, 1.5 mL) and dropped onto a quartz disk in the same procedure as for HMTT·$BiCl_3$ (**1**). The crystallites thus deposited have a slightly darker red color but similar average sizes. X-ray powder diffraction also indicated a single, crystalline phase consistent with the single-crystal structure of HMTT·$BiBr_3$ (**2**) (with strong orientation preference of the [0$\bar{1}$1] plane). The crystallites are similarly stable in air.

Solution Deposition of HETT·2BiBr$_3$ (4). HETT (3.2 mg, 0.0054 mmol), $BiBr_3$ (6.1 mg, 0.0136 mmol), and benzene (anhydrous, 1.2 mL) were handled in a similar procedure, but with the solution and the quartz disk both heated to only 90 °C. The crystallites thus deposited were significantly smaller and had a lighter red color, as compared to the above HMTT·$BiCl_3$ (**1**) and HMTT·$BiBr_3$ (**2**) crystallites. X-ray powder diffraction indicated a single, crystalline phase consistent with the single-crystal structure of HETT·2$BiBr_3$ (**4**). The crystallites are also stable in air.

Results and Discussion

Improved Synthesis of the Organic Molecules. Molecules such as 2,3,6,7,10,11-hexakis(alkylthio)triphenylenes have been widely studied for their discotic liquid crystalline properties[61−64] and as potential organic semiconductors,[34,65] and their synthesis has been widely explored. The common way of synthesis is to react 2,3,6,7,10,11-hexabromotriphenylene (HBT) with the alkylthiolate anion ($R-S^-$), which is usually generated from the corresponding alkylthiol (R−SH) and a base (like sodium hydride). As a result, to attach an organic R− group to the triphenylene core, one has to obtain the corresponding thiol compound R−SH, which is often malodorous and may not be readily available. Also, the structure of the organic R− group can substantially alter the reactivity of the thiolate group and affect its aromatic nucleophilic attack toward HBT (note: unlike the common aliphatic nucleophilic substitution, aromatic nucleophilic substitutions usually entail more stringent reaction conditions, or strong activation of the aromatic core). For example, in our attempt to synthesize 2,3,6,7,10,11-hexakis(isopropylthio)triphenylene (HiPTT) in a patented method[84] using isopropyl thiolate and HBT, severe side reactions occurred and little of the targeted product was recovered.

We have discovered an efficient and more general procedure to synthesize 2,3,6,7,10,11-hexakis(organylthio)-triphenylene molecules with a wider range of the organic R− groups. The key step in this method is the generation of the hexaanion of 2,3,6,7,10,11- triphenylenehexathiol (HTT, see Scheme 1). We have found that the HTT hexaanion can be generated in high yield by reacting HBT with an excess of sodium methylthiolate in DMEU (*N*,*N*′-dimethylethyleneurea) at an elevated temperature (e.g., 240 °C). Presumably, the methylthiolate anion first displaced the bromo group on the HBT molecule to form the thioether (CH_3-S-Ar) link with the aromatic core, which was subsequently demethylated by the excess methylthiolate anions to form dimethylthioether (CH_3SCH_3) and the triphenylene thiolate anion. Parenthetically, dealkylations of alkyl aryl thioethers by the methylthiolate anion are relatively easy reactions and have been widely reported.[85−87] The key discovery here is that, by using a vigorous reaction condition as is mentioned above, exhaustive demethylation can be achieved to generate in high yields a polycyclic aromatic system with multiple thiolate groups.

Without isolation, the HTT hexaanion can then be reacted with an appropriate alkyl halide to afford the 2,3,6,7,10,11-hexakis(alkylthio)triphenylene in near quantitative yields. This one-pot procedure thus provides a number of advantages in comparison with the above literature method. First, it replaces the various alkylthiols with the more common and easy-to-handle alkyl halides (in the current method, the sulfur atom is invariantly introduced through sodium methylthiolate,

(84) Praefcke, K.; Kohne, B.; Poules, W.; Poetsch, E. U.S. Patent 4,631,-143, 1986.
(85) Tiecco, M. *Synthesis* **1988**, 749.
(86) Testaferri, L.; Tiecco, M.; Tingoli, M.; Chianelli, D.; Montanucci, M. *Synthesis* **1983**, 751.
(87) Tiecco, M.; Tingoli, M.; Testaferri, L.; Chianelli, D.; Maiolo, F. *Synthesis* **1982,** 478.

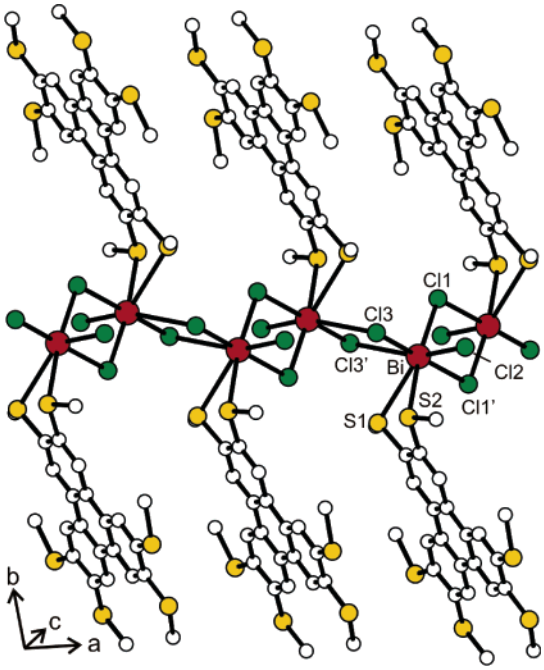

Figure 1. A hybrid chain in HMTT·$BiCl_3$ (**1**). Large red sphere, Bi; medium green, Cl; medium yellow, S; small white, C. Selected bond lengths: Bi−Cl1, 2.6659(7) Å; Bi−Cl1′, 2.9152(7) Å; Bi−Cl2, 2.4750(7) Å; Bi−Cl3, 2.5770(7) Å; Bi−Cl3′, 3.2700(8) Å; Bi−S1, 3.2478(7) Å; Bi−S2, 3.0056(7) Å.

which can be purchased as a solid at affordable prices). Second, it replaces the potentially more complicated aromatic nucleophilic substitution (between HBT and alkylthiolate) with the facile aliphatic nucleophilic substitution between the HTT anion and the alkyl halide. Moreover, various other linkages (besides the thioether linkage) can be formed from the anionic sulfur sites of the HTT hexaanion. For example, the HTT anion can be reacted with acyl halides or acid anhydrides to form the thioester linkage. In general, this procedure allows a wide range of organic groups to be readily attached to the triphenylene core and facilitates the functional modification of 2,3,6,7,10,11-hexakis(organylthio)triphenylene molecules for materials properties studies. We are further exploring the synthetic power of this discovery and plan to describe our studies in a separate publication.

Single-Crystal Structure of HMTT·$BiCl_3$ (1). This structure has been reported in a previous communication.[82] The structure (space group: $P\bar{1}$, with one $BiCl_3$ unit and one HMTT molecule in the asymmetric unit) features one-dimensional $BiCl_3$ chains, to which the HMTT ligand is periodically attached through the chelation between the Bi(III) centers and the sulfurs atoms (see Figure 1). The Bi atom is surrounded by five Cl atoms (Cl1, Cl2, Cl3, Cl1′, Cl3′) and a pair of sulfur atoms from an HMTT molecule. The coordination geometry around the Bi atom can be deconstructed into three portions. First, the Bi atom forms a trigonal pyramid with three Cl atoms (Cl1, Cl2, and Cl3) at rather short distances (Bi−Cl1, 2.67 Å; Bi−Cl2, 2.48 Å; Bi−Cl3, 2.58 Å) and with bond angles around 90° (Cl1−Bi−Cl2, 85.37 Å; Cl1−Bi−Cl3, 98.37 Å; Cl2−Bi−Cl3, 90.33 Å). Second, the Cl1′ and Cl3′ atoms form distinctly longer bonds (distances: Bi−Cl1′, 2.92 Å; Bi−Cl3′, 3.27 Å,

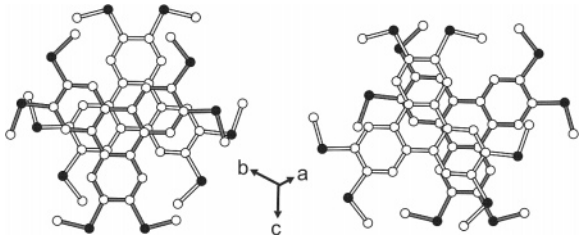

Figure 2. Two types of $\pi-\pi$ overlaps between neighboring HMTT molecules in HMTT·$BiCl_3$ (**1**) (view perpendicular to the triphenylene planes). Interplanar distances: left, 3.34 Å; right, 3.45 Å.

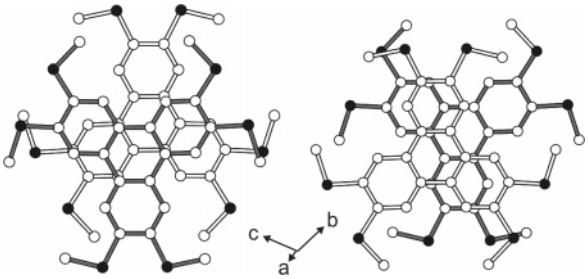

Figure 3. Two types of $\pi-\pi$ overlaps between neighboring HMTT molecules in HMTT (view perpendicular to the triphenylene planes). Interplanar distances: left, 3.43 Å; right, 3.44 Å.

Bi···Cl van der Waals distance > 3.8 Å[88]) to constitute a distorted square pyramid around the Bi^{3+} center, with Cl1 at the apex and the other four Cl atoms at the basal plane. Third, the open space opposite (i.e., trans to) the Cl1 apex is occupied by two sulfur atoms from an HMTT molecule (Bi−S lengths: 3.01 and 3.25 Å), furnishing a seven-fold coordination geometry resembling a monocapped trigonal antiprism.

The neighboring Bi coordination units share edges to form an organic−inorganic hybrid chain (i.e., two edges are shared from each Bi unit: one is that of Cl1 and Cl1′, and the other is that of Cl3 and Cl3′; see Figure 1). The hybrid chains interdigitate with one another, forming columns of the HMTT ligands based on the $\pi-\pi$ stacking interaction (see Figure S5 in the Supporting Information). Within each stack of the organic molecules, two interplanar distances alternate with each other along the stacking direction (3.34 and 3.45 Å; see Figure 2). Notice that the packing motifs of the organic molecules in the crystal structures of HMTT·$BiCl_3$ (**1**) and HMTT are very similar (compare Figure 2 to Figure 3, the corresponding interplanar distances in HMTT are 3.43 and 3.44 Å; also compare Figure S5 to Figure S6 in the Supporting Information). Overall, the crystal structure of HMTT·$BiCl_3$ (**1**) consists of chains of the $BiCl_3$ components imbedded in a matrix of the organic molecules (Figure S7).

Single-Crystal Structure of HMTT·$BiBr_3$ (2). This compound is isostructural to the above HMTT·$BiCl_3$ (**1**), featuring similar network connectivity and packing of the organic molecules. Each Bi^{3+} center is coordinated to five Br atoms (Br1, Br2, Br3, Br1′, Br3′; see Figure 4) and two sulfur atoms from an HMTT molecule, and the coordination geometry is similar to that of HMTT·$BiCl_3$ (**1**). The Bi−Br bond lengths are shown in the caption of Figure 4, and they range from 2.62 to 3.48 Å, which compare well with those in the above HMTT·$BiCl_3$ (**1**). The two Bi−S bonds are 3.03

(88) Bondi, A. J. *Phys. Chem.* **1964**, *68*, 441.

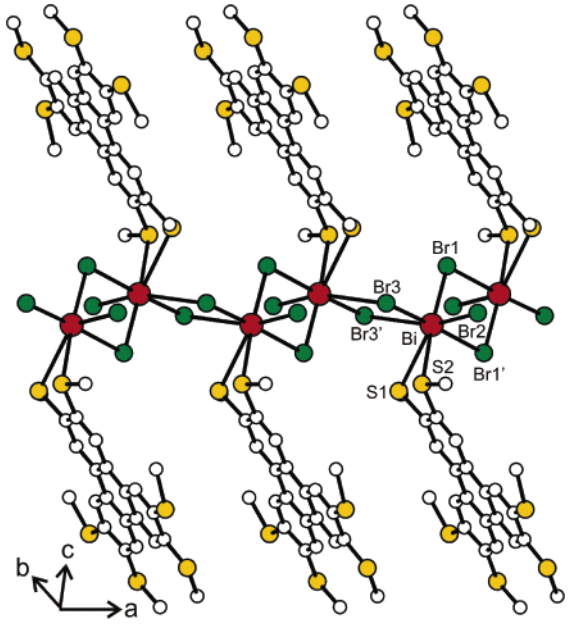

Figure 4. A hybrid chain in HMTT·$BiBr_3$ (**2**). Large red sphere, Bi; medium green, Br; medium yellow, S; small white, C. Selected bond lengths: Bi−Br1, 2.7992(6) Å; Bi−Br1′, 3.0688(6) Å; Bi−Br2, 2.6185(7) Å; Bi−Br3, 2.7168(6) Å; Bi−Br3′, 3.4788(7) Å; Bi−S1, 3.298(1) Å; Bi−S2, 3.027(1) Å.

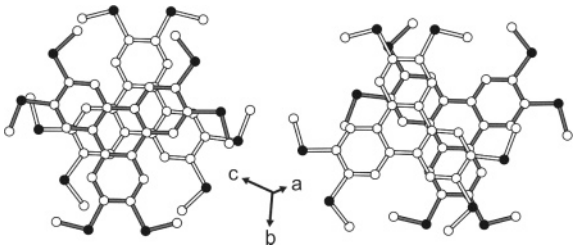

Figure 5. Two types of $\pi-\pi$ overlaps between neighboring HMTT molecules in HMTT·$BiBr_3$ (**2**) (view perpendicular to the triphenylene planes). Interplanar distances: left, 3.37 Å; right, 3.53 Å.

and 3.30 Å in lengths, which are also similar to those of HMTT·$BiCl_3$ (**1**) (3.01 and 3.25 Å).

Like in HMTT·$BiCl_3$ (**1**), the interdigitation of the neighboring composite chains (along the crystallographic *a* axis) forms stacks of HMTT molecules based on the $\pi-\pi$ interaction (Figure S8). Within each stack, two alternating interplanar distances between the neighboring HMTT molecules are found (3.37 and 3.53 Å; see also Figure 5). These interplanar distances are slightly longer than those in the HMTT·$BiCl_3$ (**1**) structure (3.34 and 3.45 Å, Figure 2), suggesting a similar but slightly weaker $\pi-\pi$ interaction in the current structure. An overview of the crystal structure (along the *a*-axis) is given in Figure S9 to illustrate the $BiBr_3$ chains being imbedded in the matrix of the organic molecules.

Single-Crystal Structure of HMTT·2$BiBr_3$ (3). This compound crystallized in the $P\bar{1}$ space group, and the asymmetric portion of the unit cell consists of one HMTT molecule and two $BiBr_3$ units. As compared to the above two structures, which contain HMTT and bismuth(III) halide in a 1:1 ratio and feature 1D coordination chains, this structure contains HMTT and $BiBr_3$ in a 1:2 ratio and features a 2D coordination network. As shown in Figure 6, the 2D network is based on $BiBr_3$ chains cross-linked by the organic

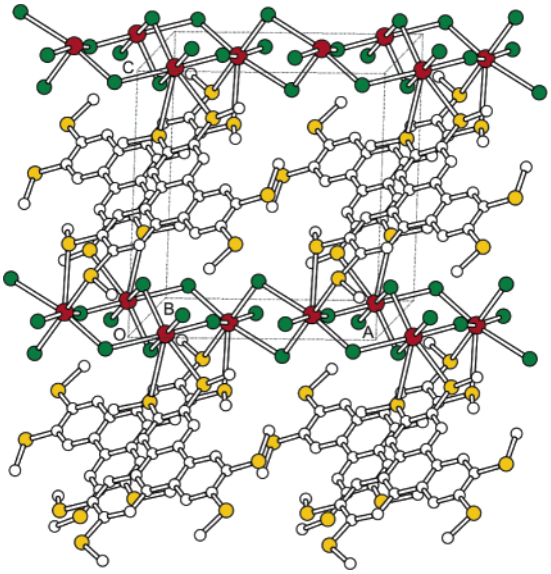

Figure 6. A hybrid 2D network in the crystal structure of HMTT·2$BiBr_3$ (**3**). Large red sphere, Bi; medium green, Br; medium yellow, S; small white, C.

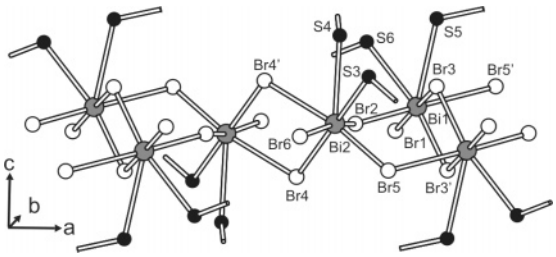

Figure 7. A portion of the $BiBr_3$ chain in HMTT·2$BiBr_3$ (**3**) with atom labeling. Selected bond lengths: Bi1−Br1, 2.6418(8) Å; Bi1−Br2, 2.6447-(8) Å; Bi1−Br3, 3.2894(8) Å; Bi1−Br3′, 2.7172(8) Å; Bi1−Br5′, 3.2973-(8) Å; Bi2−Br2, 3.4024(8) Å; Bi2−Br4, 2.7480(7) Å; Bi2−Br4′, 3.2630(8) Å; Bi2−Br5, 2.7165(8) Å; Bi2−Br6, 2.6154(7) Å; Bi1−S5, 3.446(2) Å; Bi1−S6, 3.117(2) Å; Bi2−S3, 3.099(2) Å; Bi2−S4, 3.312(2) Å.

molecules (two of the three pairs of sulfur atoms are bonded to the $BiBr_3$ chains, while the other one stays unbonded).

The coordination geometry around the Bi^{3+} atoms as well as the connectivity of the $BiBr_3$ chain is shown in Figure 7. Like HMTT·$BiCl_3$ (**1**) and HMTT·$BiBr_3$ (**2**), the coordination geometries around Bi1 and Bi2 atoms can also be deconstructed into three components. First, the Bi1 atom is coordinated to three Br atoms (Br1, Br2, and Br3′) to form the trigonal pyramid (bond angles, Br1−Bi1−Br2, 92.74°; Br1−Bi1−Br3′, 92.32°; Br2−Bi1−Br3′, 92.18°). Second, the addition of the Br3 and Br5′ atoms constitutes a distorted square pyramid (with Br3′ at the apex). Third, the open space opposite the Br3′ apex is occupied by the two sulfur atoms from an HMTT molecule, completing the seven-fold coordination geometry. Similarly, the Bi2 atom is first bonded to Br4, Br5, Br6 to form the trigonal pyramid (bond angles: Br4−Bi2−Br5, 90.82°; Br4−Bi2−Br6, 89.82°; Br5−Bi2−Br6, 92.54°); the addition of the Br2 and Br4′ furnishes a distorted square pyramid (with Br4 at the apex); the space opposite the Br4 apex was occupied by two sulfur atoms (S3 and S4) to complete the seven-fold coordination.

The connectivity of the bismuth(III) bromide chain can be deconstructed into dimers of the Bi1 and Bi2 coordination spheres. Both the Bi1 and the Bi2 dimers are centrosymmetric, with the Bi dimer formed by the sharing of Br3 and

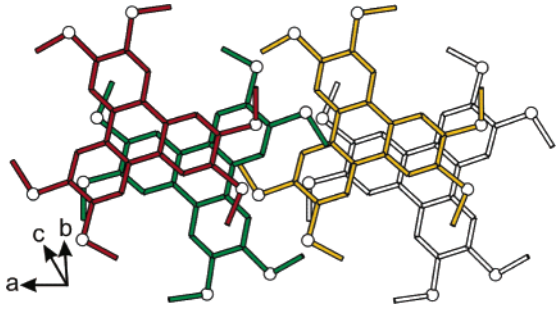

Figure 8. Four neighboring HMTT molecules in HMTT·2BiBr$_3$ (**3**) showing the $\pi-\pi$ overlaps (view perpendicular to the triphenylene planes). White sphere, S. The coloring highlights relative heights of the molecules (from top to bottom): red, green, yellow, and white.

Br3′ atoms and the Bi2 dimer by the sharing of the Br4 and Br4′ atoms (Figure 7). The Bi1 and Bi2 dimers are then connected into a chain (with the Bi1, Bi2 dimers alternating one another) by sharing the Br2 and Br5 atoms (see also Figure 7). Notably, the Bi1 dimer provides a larger cross-section to the chain than does the Bi2 dimer, because the longest dimension (i.e., along the two Bi atoms) of Bi1 dimer spans across the chain (almost at a right angle to the chain direction), whereas the two Bi atoms of Bi2 dimer lie along the chain. Also, as compared to the BiBr$_3$ chain of the above HMTT·BiBr$_3$ (**2**) (where all of the Bi centers lie along the chain), the Bi1 dimers here impart to its inorganic chain an overall lateral dimension larger than that of HMTT·BiBr$_3$ (**2**).

The BiBr$_3$ chains are connected into a 2D network (a layer) by the HMTT molecules, as is shown in Figure 6 and Figure S10. No significant $\pi-\pi$ interaction exists between the organic molecules within the same layer (closest intermolecular C···C contact being longer than 3.8 Å). Pairs of closely interacting HMTT molecules are, however, found across the neighboring layers, with interplanar distance of 3.53 Å (see Figure S10b for the packing of the neighboring layers along the *b* axis; see Figure 8 for a projection of the neighboring molecules within the triphenylene stacks of Figure S10b). In comparison to the previous structures, the interplanar distance here is longer and the face-to-face overlap (see Figure 8) of the two molecules is smaller; also the $\pi-\pi$ stacking only organizes the molecules into discrete pairs, instead of the extended columns of organic molecules in the above three structures. The $\pi-\pi$ interactions between the organic molecules, therefore, appear to be significantly weaker in this structure.

Single-Crystal Structure of HETT·2BiBr$_3$ (4). This structure is in the space group $P\bar{1}$, and the asymmetric portion of the unit cell consists of one HETT molecule and two BiBr$_3$ fragments. As shown in Figure 9, the Bi1 atom is coordinated to four Br atoms and two sulfur atoms, with Br1, Br2, and Br3′ atoms forming the persistent trigonal pyramidal geometry around the Bi1 center (see Figure 9 for bond lengths; bond angles: Br1−Bi1−Br2, 92.02°; Br1−Bi1−Br3′, 93.86°; Br2−Bi1−Br3′, 102.82°). Two sulfur atoms (S5 and S6, Figure 9) from an HETT molecule furnish a distorted square pyramidal geometry around the Bi1 atom, with Br1 at the apex, and S5, S6, Br2, and Br3′ atoms in the basal plane. Finally, Br3 approaches the Bi1 center from opposite the Br1 apex and completes a distorted octahedral geometry around the Bi1 atom.

The Bi2 is first bonded to atoms Br4, Br5, and Br6 to form the conservative trigonal pyramid (bond angles: Br4−Bi2−Br5, 91.83°; Br4−Bi2−Br6, 94.05°; Br5−Bi2−Br6, 96.38°); two sulfur atoms (S3 and S4) then provide a distorted square pyramid (with Br4 at the apex, and S3, S4, Br5, Br6 at the basal plane); finally, Br1 and Br2 approach Bi2 from opposite the Br4 apex to form rather weak secondary bonds (Bi−Br distances: Bi2−Br1, 3.64 Å; Bi2−Br2, 3.76 Å) to complete a seven-coordinated geometry resembling a monocapped trigonal antiprism.

Unlike the previous structures, where the bismuth halide components form extended structures (1D or 2D), the BiBr$_3$ component here forms isolated (0D) units of Bi$_4$Br$_{12}$, which can be considered quasi-tetrameric due to the two notably long bridging Bi−Br bonds in the structure (Bi2−Br1, 3.64 Å; Bi2−Br2, 3.76 Å; see Figure 9). The quasi-tetramer Bi$_4$Br$_{12}$ is centrosymmetric, and its central portion consists of two Bi1 coordination units sharing the Br3 and Br3′ atoms. The Bi1 dimer then interacts with two Bi2 coordination units (one on each side, e.g., by sharing the Br1 and Br2 atoms; see Figure 9) to complete the overall quasi-tetrameric structure. The Bi$_4$Br$_{12}$ quasi-tetrameric units are linked into a quasi-one-dimensional coordination network by the organic molecules as is also shown in Figure 9. The quasi-1D networks interact with one another through rather weak interactions between the triphenylene units (interplanar distance: 3.82 Å, the shortest C···C contacts are marked in Figure S11 of the Supporting Information). No other significant $\pi-\pi$ interactions between the organic molecules were observed.

Briefly, we now comment on network dimensionality. Due to the rather wide and continuous variation of Bi−X distances observed in the current compounds, the distinction among quasi-1D, 1D, and other dimensionalities could be rather fuzzy. Our definition here is solely based on comparing the bonding features among the individual compounds, with the purpose of offering a nicer distinction of network connectivity within these flexible Bi−X systems. For example, we have chosen to define the BiBr$_3$ chains in the above HMTT·BiBr$_3$ (**2**) and HMTT·2BiBr$_3$ (**3**) as 1D, mainly because the bridging Bi−Br bonds therein (below 3.48 Å) are considerably shorter than the ones in the BiBr$_3$ chains of HETT·2BiBr$_3$ (**4**) (which are termed quasi-1D in this comparative sense). A more systematic comparison of the bridging Bi−X lengths is also included in Table 2.

Single-Crystal Structure of HiPTT·2BiBr$_3$·C$_7$H$_8$ (5). This crystal structure is in the space group of $P2_1/c$ and contains two HiPTT molecules, four BiBr$_3$ fragments, together with two toluene molecules (enclathrated solvent molecules) in the asymmetric portion of the unit cell. The crystal structure features isolated (0D) hybrid units in which two HiPTT molecules are bound together in a face-to-face manner (interplanar distance: 3.49 Å) by three bismuth(III) bromide fragments (see Figure 10). Two of the inorganic fragments each consist of one Bi atom and three Br atoms forming a trigonal pyramid (e.g., Bi2, Br4, Br5, Br6), and the third fragment consists of two edge-sharing BiBr$_3$ trigonal

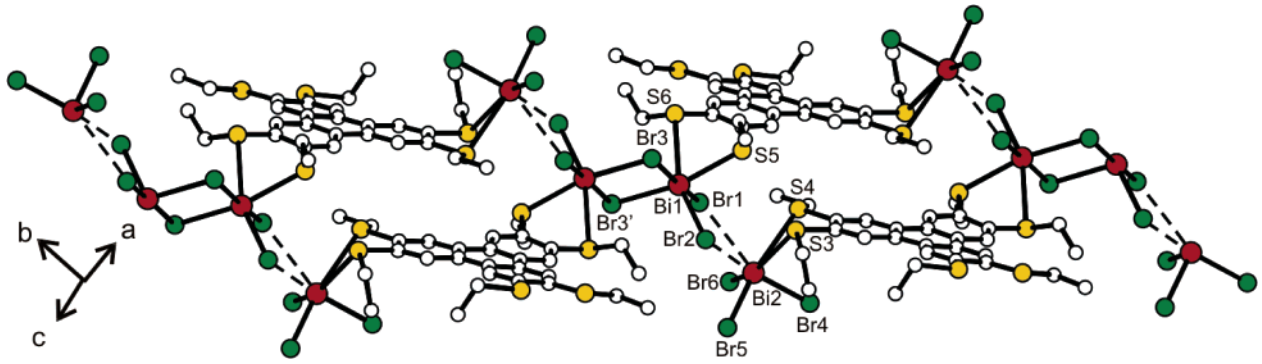

Figure 9. The quasi-1D coordination network in the crystal structure of HETT·2BiBr$_3$ (**4**). Large red sphere, Bi; medium green, Br; medium yellow, S; small white, C. Elongated Bi−Br bonds are shown in dashed lines. Selected bond lengths: Bi1−Br1, 2.671(2) Å; Bi1−Br2, 2.675(2) Å; Bi1−Br3, 3.105(1) Å; Bi1−Br3′, 2.854(1) Å; Bi2−Br1, 3.636(1) Å; Bi2−Br2, 3.760(2) Å; Bi2−Br4, 2.619(1) Å; Bi2−Br5, 2.652(1) Å; Bi2−Br6, 2.659(1) Å; Bi1−S5, 2.908(2) Å; Bi1−S6, 3.043(3) Å; Bi2−S3, 3.318(2) Å; Bi2−S4, 3.219(2) Å.

Table 2. Selected Structural Parameters and Electronic Properties for HMTT·2BiBr$_3$ (3), HMTT·BiBr$_3$ (2), HMTT·BiCl$_3$ (1), HETT·2BiBr$_3$ (4), HiPTT·2BiBr$_3$·C$_7$H$_8$ (5), and HMTT

compounds	network dimensionality	band gap (eV)	Bi−S distances (Å)	Bi−X distances (Å)[b]	interplanar $\pi-\pi$ distance (Å)
3	2D	1.64	3.12, 3.45 3.10, 3.31	(2.64, 3.40) (2.72, 3.30) (2.72, 3.29)	3.53[c]
2	1D	1.75	3.03, 3.30	(2.80, 3.07) (2.72, 3.48)	3.37, 3.53[d]
1	1D	1.82	3.01, 3.25	(2.67, 2.92) (2.58, 3.27)	3.34, 3.45[d]
4	Quasi-1D	1.97	2.91, 3.04 3.22, 3.32	(2.67, 3.64) (2.68, 3.76) (2.85, 3.10)	3.82[c]
5	0D	2.18	3.01, 3.12 3.29, 3.50[a]	(2.69, 3.31) (2.76, 3.22)	3.49[c]
HMTT	0D	2.98	none	none	3.44, 3.43[d]

[a] Selected data; see Figure 10 for more Bi−S bond lengths. [b] For bridging X (Br or Cl) atoms (the two Bi−X lengths for each X atom are grouped in parentheses); see the figure captions for the Bi−X lengths for terminal X atoms. [c] The triphenylene cores are stacked into discrete pairs in this structure. [d] The triphenylene cores are stacked into infinite columns in this structure.

pyramids (i.e., one from Bi1, Br1, Br2, Br3 and the other from Bi4, Br10, Br11, Br12). Each inorganic fragment interacts with a pair of sulfur atoms from each organic molecule (i.e., four sulfur atoms for each fragment), which completes a seven-fold coordination geometry around Bi1, Bi2, and Bi3 (Bi4 is not directly bonded to the organic molecule).

The overall coordination geometries of Bi1, Bi2, and Bi3 resemble a monocapped trigonal antiprism. In a rough observation, three Br atoms first bond to the Bi center (e.g., Br4, Br5, Br6, and Bi2) at short distances (between 2.60 and 2.80 Å) to form the common trigonal pyramid; the open space opposite the three Br atoms is occupied by two pairs of the sulfur atoms to complete the coordination around the Bi center. Upon closer examination, however, one distinguishes a distorted square pyramid around each of the Bi1, Bi2, and Bi3 atoms; that is to say, around the Bi3 atom, S6, S16, Br7, and Br9 constitute the basal plane, while Br8 forms the apex; around the Bi2 atom, S13, S14, Br4, and Br6 form the base and Br5 the apex; around the Bi1 atom, S1, S2, Br1, and Br2 form the base and Br3 the apex (Figure 10). Similar square pyramids are also found in the previous HETT·2BiBr$_3$ (**4**). The open space opposite the apex of the square pyramid is then occupied by the remaining two sulfur atoms to furnish the seven-fold coordination.

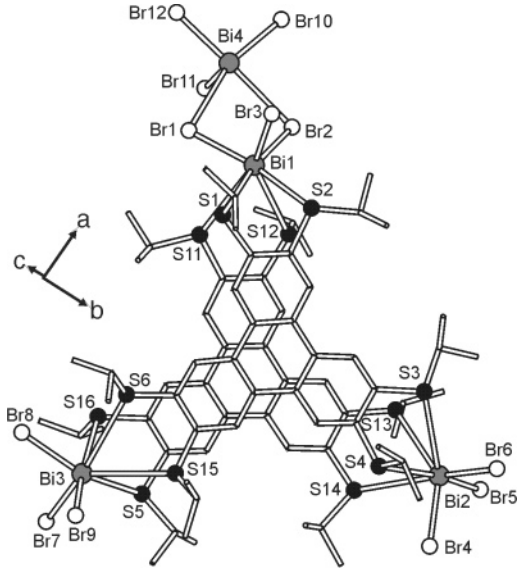

Figure 10. The isolated (0D) coordination unit (with two HiPTT molecules, two BiBr$_3$, and one Bi$_2$Br$_6$ fragment) in HiPTT·2BiBr$_3$·C$_7$H$_8$ (**5**). Large gray spheres, Bi; small white, Br; small black, S. Selected bond lengths: Bi1−Br1, 2.688(2) Å; Bi1−Br2, 2.756(2) Å; Bi1−Br3, 2.621(2) Å; Bi2−Br4, 2.609(2) Å; Bi2−Br5, 2.665(2) Å; Bi2−Br6, 2.608(2) Å; Bi3−Br7, 2.627(2) Å; Bi3−Br8, 2.625(3) Å; Bi3−Br9, 2.661(3) Å; Bi4−Br1, 3.314-(2) Å; Bi4−Br2, 3.218(2) Å; Bi4−Br10, 2.646(2) Å; Bi4−Br11, 2.580(3) Å; Bi4−Br12, 2.610(2) Å; Bi1−S1, 3.009(4) Å; Bi1−S2, 3.124(4) Å; Bi1−S11, 3.495(4) Å; Bi1−S12, 3.291(4) Å; Bi2−S3, 3.476(4) Å; Bi2−S4, 3.150(4) Å; Bi2−S13, 3.355(4) Å; Bi2−S14, 3.451(4) Å; Bi3−S5, 3.248-(4) Å; Bi3−S6, 3.382(4) Å; Bi3−S15, 3.534(4) Å; Bi3−S16, 3.146(4) Å.

The Bi4 atom is bonded to five Br atoms (Br1, Br2, Br10, Br11, Br12), but not to any sulfur atoms. The overall geometry is a distorted square pyramid. Among the Br atoms, Br10, Br11, and Br12 (Bi−Br distances from 2.58 to 2.65 Å; see also Figure 10) constitute the common trigonal pyramid with the Bi4 atom. The Br1 and Br2 atoms are more remote from the Bi4 center (distances: Bi4−Br1, 3.31 Å; Bi4−Br2, 3.22 Å), and they lie in roughly the same plane (i.e., the basal plane of the square pyramid) as Br10 and Br12. Unlike the other cases, the open space opposite the apex (Br11) is not occupied and the total coordination number stays at five. The packing of the individual hybrid units is shown in Figure S12. No significant $\pi-\pi$ interactions are found across the hybrid units.

Correlation between Molecular and Crystal Structures. Taken together, the above hybrid coordination networks feature rather diverse compositions and network dimension-

alities, covering the 2D structure of HMTT·2$BiBr_3$ (**3**), the 1D systems of HMTT·$BiBr_3$ (**2**) and HMTT·$BiCl_3$ (**1**), the quasi-1D HETT·2$BiBr_3$ (**4**), and the 0D HiPTT·2$BiBr_3$·C_7H_8 (**5**). Due to the composite nature of the networks, their dimensionalities are determined by the structure of the inorganic fragments as well as the coordinating pattern of the organic ligand. Apparently, an extended (vs isolated) structure of the BiX_3 component is conducive to a higher-dimensional hybrid net, and an organic ligand with more sulfur sites bonded to Bi^{3+} centers may also increase the dimensionality of the hybrid net. For example, the 2D network of HMTT·2$BiBr_3$ (**3**) is based on infinite chains of $BiBr_3$ interconnected by two pairs of sulfur atoms from each HMTT molecule, while in HMTT·$BiBr_3$ (**2**), each HMTT molecule is bonded to the $BiBr_3$ chain through only one pair of sulfur atoms (and therefore the hybrid net remains 1D). Similarly, the 0D structure of HiPTT·2$BiBr_3$·C_7H_8 (**5**) features isolated dimers and monomers of the $BiBr_3$ component.

It appears at this point that the dimensionality of the BiX_3 component tends to be lowered by enlarging the alkyl side chains on the organic molecule, for example, HMTT·$BiBr_3$ (**2**) contains chains of $BiBr_3$, HETT·2$BiBr_3$ (**4**) quasi-tetrameric units of $BiBr_3$, and HiPTT·2$BiBr_3$·C_7H_8 (**5**) dimers and monomers of $BiBr_3$. We suspect that the overall structures of these hybrid compounds could be deconstructed into several chemically distinct components (e.g., the aromatic triphenylene units, the relatively polar $BiBr_3$ component, and the nonpolar aliphatic side chains), and the study of the interfaces among these components might provide a better understanding of the crystal structures. Conceivably, ever larger side chains would sufficiently reduce the volume fraction of the BiX_3 component and force it to form into isolated fragments. Further studies are, however, needed to examine this idea, although the relations between interface topology and crystal structure have recently been studied for essentially two-component systems.[89−91]

Structure−Property Relations. In contrast to the almost colorless crystals of the organic compounds (i.e., HMTT, HETT, and HiPTT) and the bismuth halides (i.e., $BiCl_3$ and $BiBr_3$), the hybrid compounds are distinctly colored, ranging from the very dark red of HMTT·2$BiBr_3$ (**3**) to the lighter orange-yellow color of HiPTT·2$BiBr_3$·C_7H_8 (**5**). Optical absorption measurements (see Experimental Section for more detail) provide a more quantitative assessment of the electronic band gaps of the hybrid semiconductors. As is shown in Figure 11, the optical band gaps of the above compounds increase in the following order: HMTT·2$BiBr_3$ (**3**) (1.642 eV), HMTT·$BiBr_3$ (**2**) (1.753 eV), HMTT·$BiCl_3$ (**1**) (1.817 eV), HETT·2$BiBr_3$ (**4**) (1.973 eV), HiPTT·2$BiBr_3$·C_7H_8 (**5**) (2.177 eV), HMTT (2.983 eV). For more comparison, similar diffuse reflectance measurements indicate the band gaps of $BiCl_3$ and $BiBr_3$ to be 3.366 and 2.662 eV, respectively (see Figure S13 in the Supporting Information).

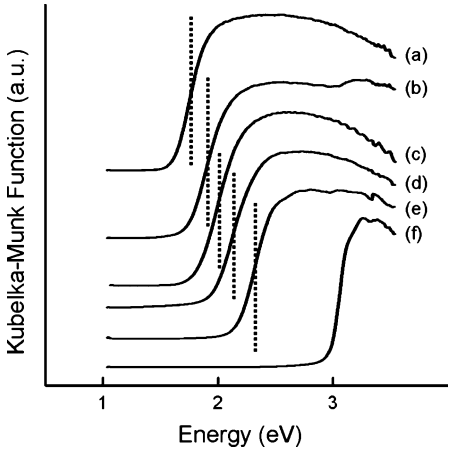

Figure 11. Room-temperature optical absorption spectra for solid samples of (a) HMTT·2$BiBr_3$ (**3**); (b) HMTT·$BiBr_3$ (**2**); (c) HMTT·$BiCl_3$ (**1**); (d) HETT·2$BiBr_3$ (**4**); (e) HiPTT·2$BiBr_3$·C_7H_8 (**5**); and (f) HMTT. Dotted lines highlight the relative positions of the absorption edges.

The smaller band gaps (and thus the darker coloring) of the hybrid systems indicate that substantial electronic interaction may exist between the bismuth(III) halide components and the organic molecules. Conceivably, there exist three types of interactions, which may significantly affect the electronic properties of the hybrid compounds: the coordination (chelation) bonds between the 1,2-bis(alkylthio) groups and the Bi^{3+} centers, the coordination bonds between the halide anions and the Bi^{3+} centers, and the $\pi-\pi$ stacking force among the aromatic molecules. A survey of the crystal structures and the corresponding electronic properties suggests that, within these hybrid networks, the Bi(III)−S and the Bi(III)−X coordination bonds are substantially more important determinants of the solid-state electronic properties (e.g., band gaps) than the $\pi-\pi$ overlaps between the organic molecules. To assist the following discussion of this point, we use Table 2 to summarize the electronic band gap data and the key structural parameters of the hybrid semiconductors (together with the organic compound HMTT).

A strong indication that the Bi−S and Bi−X coordination bonds are major determinants for the electronic properties comes from comparing the organic compound HMTT with the hybrid HMTT·2$BiBr_3$ (**3**), which respectively present the high end and low end of the band gaps listed in Table 2. In the crystal structure of HMTT, the $\pi-\pi$ stacking organizes the organic molecules into one-dimensional columns: the interplanar distances (3.43 and 3.44 Å) are rather short, and the overlap between neighboring molecules is quite large (see Figure 3). In fact, it is reasonable to consider the $\pi-\pi$ stacking force as the major intermolecular interaction for this planar polycyclic aromatic compound. By contrast, the $\pi-\pi$ interaction in the hybrid HMTT·2$BiBr_3$ (**3**) appears to be significantly weakened: the interplanar distance is elongated to 3.53 Å; moreover, the $\pi-\pi$ interaction only organizes the organic molecules into isolated pairs (instead of the 1D columns in HMTT). The small band gap of HMTT·2$BiBr_3$ (**3**) can thus be ascribed to the rather extensive Bi−S and Bi−Br coordination bonding in the crystal structure (which results in a two-dimensional coordination network). Similarly, in the hybrids of HETT·2$BiBr_3$ (**4**) and HiPTT·2$BiBr_3$·C_7H_8 (**5**), the $\pi-\pi$ interaction also organizes the organic

(89) Mallik, A. B.; Lee, S.; Tran, L.; Lobkovsky, E. B. *Cryst. Growth Des.* **2003**, *3*, 467.
(90) Xu, Z.; Kiang, Y.-H.; Lee, S.; Lobkovsky, E. B.; Emmott, N. *J. Am. Chem. Soc.* **2000**, *122*, 8376.
(91) Xu, Z.; Lee, S.; Lobkovsky, E. B.; Kiang, Y.-H. *J. Am. Chem. Soc.* **2002**, *124*, 121.

molecules into isolated pairs (not a continuous column as in HMTT). Notice also that the interplanar distances between neighboring molecules in these two hybrids [3.82 Å for HETT·$2BiBr_3$ (**4**) and 3.49 Å for HiPTT·$2BiBr_3$·C_7H_8 (**5**)] are significantly longer than the ones in HMTT. The fact that both HETT·$2BiBr_3$ (**4**) and HiPTT·$2BiBr_3$·C_7H_8 (**5**) exhibit smaller band gaps than HMTT further indicates the Bi−S and Bi−X coordination bonds as the principal cause for the reduction of the band gaps of the hybrid systems.

Next, we demonstrate that the smaller band gaps of the hybrid systems (as compared to the HMTT compound) are resulted from both the Bi−S interactions and the intervening Bi−X bonds. In particular, we place emphasis on the Bi−X bonds, so as to highlight the extended nature of the electronic interaction between the organic π-system and the Bi−X component. Consider first HiPTT·$2BiBr_3$·C_7H_8 (**5**). All three pairs of alkylthio groups in this structure are bonded to Bi(III) centers (whereas in the other four hybrids, only one or two pairs of alkylthio groups are bonded to bismuth atoms), and the strength of the Bi−S bonds (the shortest being 3.01 and 3.12 Å) compares well with those in the other hybrids (see Table 2). Compound HiPTT·$2BiBr_3$·C_7H_8 (**5**) therefore features the most intense interaction between the organic molecules and the Bi^{3+} atoms. However, it is also HiPTT·$2BiBr_3$·C_7H_8 (**5**) that exhibits the largest band gap (i.e., the weakest electroactivity) among the hybrid compounds (see Table 2), suggesting that the Bi−S interactions alone do not suffice to account for the electroactivities among the hybrid compounds. In other words, the Bi−X bonds may also play a role in reducing the band gaps of the hybrid networks. Indeed, the large band gap of HiPTT·$2BiBr_3$·C_7H_8 (**5**) seems to arise from the terminating $BiBr_3$ fragments that seal off the organic molecules into isolated complex units (0D) (see Figure 10); whereas in the other hybrid systems, the Bi−X components serve as bridging units that interconnect the organic molecules into extended networks. Overall, within these hybrid systems, there exists a rather clear correlation between the band gaps and the dimensionalities of the hybrid coordination networks (based on both the Bi−S bonds and the Bi−X bonds); higher-dimensional networks generally lead to smaller electronic band gaps (see Table 2). The above data indicate that the intervening Bi−X bonds do not constitute barriers that localize the electronic interactions between the organic π-systems and the individual Bi(III) centers (mediated by the Bi−S chelation bonds); instead, they provide electroactive connections across the organic π-systems and effectively influence the electronic properties of the hybrid networks.

The impact of the bismuth halide components on the electronic properties of the hybrid networks is also illustrated in a comparison between HMTT·$BiBr_3$ (**2**) and HMTT·$BiCl_3$ (**1**). Compounds **2** and **1** are isostructural, featuring close similarity in the connectivity of the hybrid networks (see Figures 1 and 4) as well as the packing of the organic molecules (see Figures 2 and 5). Notice, in particular, that both the Bi−S bonds (3.03 and 3.30 Å) and the $\pi-\pi$ interactions (interplanar distances: 3.37 and 3.53 Å) in HMTT·$BiBr_3$ (**2**) seem to be slightly weaker than those of HMTT·$BiCl_3$ (**1**) (see Table 2), and yet the band gap of HMTT·$BiBr_3$ (**2**) (1.75 eV) is smaller than that of HMTT·$BiCl_3$ (**1**) (1.82 eV). It therefore appears that the Bi−Br component in HMTT·$BiBr_3$ (**2**) overcompensates for the slightly weaker Bi−S bonds and $\pi-\pi$ interactions and results in a reduction of the electronic band gap [in comparison with HMTT·$BiCl_3$ (**1**)]. As would be expected, the bromine atom is a heavier and softer congener of the chlorine atom, and its higher-energy 4p electrons may be responsible for reducing the band gap in HMTT·$BiBr_3$ (**2**) as compared to the chlorine counterpart HMTT·$BiCl_3$ (**1**).

The $\pi-\pi$ overlap is usually considered a major interaction between large aromatic molecules. Such intermolecular interaction effectively influences the packing of the molecules as well as the electronic properties of the molecular crystals. By comparison, the above discussions indicate that, in the newly synthesized hybrid systems, higher dimensionalities of the coordination network uniformly result in smaller electronic band gaps, suggesting the Bi−S and Bi−X coordination bonds as potentially significant determinants of the solid-state electronic properties (although ligand coordination modes such as bond angles could also potentially perturb the electronic properties of the organic−inorganic composites). In other words, significant electronic interactions may have been installed between the organic π-systems and the intervening BiX_3 moieties, which effectively integrate the individual molecules into hybrid semiconductive networks. It is reasonable to expect that charge transport in these hybrid systems could follow the pathways of the coordination framework, thus providing a potentially effective mechanism for improving carrier mobility across organic molecules. In this regard, the extended structures of HMTT·$2BiBr_3$ (**3**) (2D), HMTT·$BiBr_3$ (**2**) (1D), and HMTT·$BiCl_3$ (**1**) (1D) offer particularly promising candidates for conductance and charge carrier mobility tests. Such ongoing studies are aimed to provide direct evidence for the conductivity of these coordination compounds, and to further elucidate the transport mechanisms in such hybrid solid-state materials, as such mechanisms could be potentially complex, and the conventional band structure/band gap depiction may not be the most reliable indication of how these compounds will perform in the real device situations.

Solution Processing. Finally, to further illustrate the potential use of these hybrid semiconductors in device fabrications, we present some preliminary results from solution processing tests, with emphasis on the ones with extended structures [e.g., HMTT·$2BiBr_3$ (**3**), HMTT·$BiCl_3$ (**1**), HMTT·$BiBr_3$ (**2**), and HETT·$2BiBr_3$ (**4**)]. In particular, highly crystalline, single-phase samples of HMTT·$BiCl_3$ (**1**), HMTT·$BiBr_3$ (**2**), and HETT·$2BiBr_3$ (**4**) have been deposited from heated aromatic solutions onto quartz disks. Figure 12 (pattern a) shows the X-ray powder diffraction pattern observed from a solution-processed sample of HMTT·$BiCl_3$ (**1**) (deposited from a hot 1,2-dichlorobenzene solution onto a quartz disk). The observed pattern agrees with the ones calculated from the single-crystal structure and features distinct orientation preference of the $[0\bar{1}1]$ direction for the solution-deposited sample (see patterns b and c in Figure 12). Such orientation preference of the crystallites reflects easy cleavage along the $[0\bar{1}1]$ plane: as is seen in the crystal

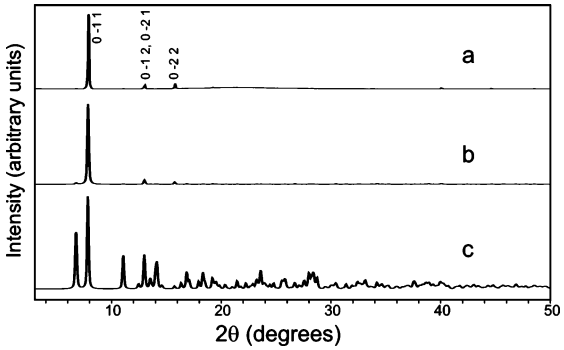

Figure 12. X-ray diffraction patterns (Cu Kα, $\lambda = 1.5418$ Å) of HMTT·$BiCl_3$ (**1**): (a) observed for a solution-deposited sample; (b) calculated from the single-crystal structure with orientation preference for the [0$\bar{1}$1] plane; and (c) calculated from the single-crystal structure with random orientation of crystallites.

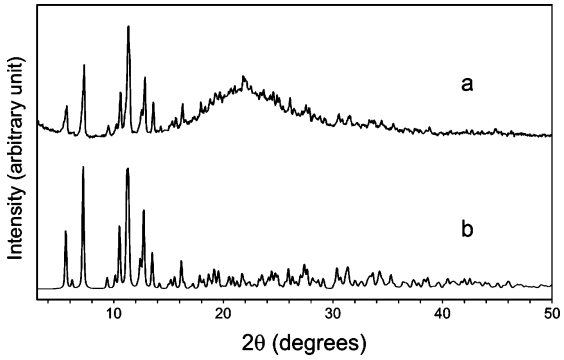

Figure 13. X-ray diffraction patterns (Cu Kα, $\lambda = 1.5418$ Å) of HETT·$2BiBr_3$ (**4**): (a) observed for a solution-deposited sample; and (b) calculated from the single-crystal structure with random orientation of crystallites.

structure of HMTT·$BiCl_3$ (**1**) (see Figure S7 in the Supporting Information), stronger $\pi-\pi$ stacking and coordination bonding are organized within 2D domains parallel to the [0$\bar{1}$1] plane, and the weak van der Waals gap occurs along the [01$\bar{1}$] plane. Similar results were obtained in the solution processing studies of the isostructural HMTT·$BiBr_3$ (**2**), and they are presented in Figure S14 of the Supporting Information. Attempts to deposit crystallites of HMTT·$2BiBr_3$ (**3**) from hot 1,2-dichlorobenzene solutions (e.g., with HMTT and $BiBr_3$ in 1:2, 1:3, or even higher ratios), however, only yielded HMTT·$BiBr_3$ (**2**) as the crystalline product, indicating the much faster formation of HMTT·$BiBr_3$ (**2**) under these specific experimental conditions. Further exploration of the experimental conditions is therefore needed to access solution-processed samples of compound HMTT·$2BiBr_3$ (**3**).

Highly crystalline, single-phase solid samples of compound HETT·$2BiBr_3$ (**4**) can be deposited from a hot benzene solution. The X-ray diffraction pattern of the solution-processed sample is consistent with the single-crystal structure of HETT·$2BiBr_3$ (**4**) (see Figure 13). No obvious orientation preference is observed for the solution-processed sample, which is consistent with the lack of a distinct cleavage plane (e.g., parallel to certain van der Waals gap) in the crystal structure of HETT·$2BiBr_3$ (**4**) [see Figures S15 and S16 in the Supporting Information for additional figures of HETT·$2BiBr_3$ (**4**)].

Acknowledgment. We thank George Washington University's University Facilitating Fund and donors of the American Chemical Society Petroleum Research Fund for partial support of this research. Z.X. is a recipient of the 2004 Ralph E. Powe Junior Faculty Enhancement Award. We also thank the X-ray Structural Characterization Laboratory at the Chemistry Department supported by the University of Massachusetts and the National Science Foundation (grant CHE-9974648), and Dr. A. Chandrasekaran for X-ray single-crystal data collection, structure solution, and refinement for compounds HMTT·$BiBr_3$ (**2**), HMTT·$2BiBr_3$ (**3**), HETT·$2BiBr_3$ (**4**), and HiPTT·$2BiBr_3$·C_7H_8 (**5**). We thank Dr. David B. Mitzi for helpful discussions on the manuscript.

Supporting Information Available: Full crystallographic data in CIF format for compounds HMTT·$BiBr_3$ (**2**), HMTT·$2BiBr_3$ (**3**), HETT·$2BiBr_3$ (**4**), and HiPTT·$2BiBr_3$·C_7H_8 (**5**). Additional figures of the crystal structure of HMTT·$BiCl_3$ (**1**) and HETT·$2BiBr_3$ (**4**). X-ray powder diffraction patterns for bulk samples of HMTT·$BiBr_3$ (**2**), HMTT·$2BiBr_3$ (**3**), HETT·$2BiBr_3$ (**4**), HiPTT·$2BiBr_3$·C_7H_8 (**5**), and a drop-cast sample of HMTT·$BiBr_3$ (**2**). Diffuse reflectance spectra of $BiCl_3$ and $BiBr_3$ (PDF). This material is available free of charge via the Internet at http://pubs.acs.org.

CM050377+